SAND2019-4854C

50th International Annual Conference of the Fraunhofer ICT
Convention Center, Karlsruhe, Germany (Jun 25-28, 2019)

A "UNIVERSAL" COOKOFF MODEL FOR EXPLOSIVES

Michael L. Hobbs, Michael J. Kaneshige, William W. Erikson
Sandia National Laboratories*
Albuquerque, New Mexico 87185 USA

Abstract

Over the past decade, we have been developing cookoff models for various explosives based on the Sandia Instrumented Thermal Ignition (SITI) experiment. These models describe cookoff from the pristine state to ignition, but do not predict the post-ignition violence of the event. Our models predict ignition time, spatial temperatures, and pressurization rates. We have observed that our cookoff models have similarities that are amenable to a universal cookoff model that can be used for most explosives. We present this universal cookoff model in the current work and apply the model to four unique explosives.

Introduction

Cookoff describes the thermal decomposition, subsequent ignition, and violent response of energetic materials exposed to high temperatures produced from accidents such as fire. Preignition timescales range from seconds to hours. In contrast, post-ignition events leading to violent responses are much faster with timescales on the order of milliseconds. Exothermic decomposition produces energy that is dissipated by conduction, convection, and radiation. If the internally generated energy is not dissipated fast enough, the energetic material self-heats catastrophically leading to thermal runaway or ignition. The subsequent mode of burning (conductive, convective, or volumetric) and the amount of confinement determines the violence of the event, which can range from a benign pressure rupture to a violent event such as

*Sandia National Laboratories is a multi-mission laboratory managed and operated by National Technology and Engineering Solutions of Sandia, LLC., a wholly owned subsidiary of Honeywell International, Inc., for the U.S. Department of Energy's National Nuclear Security Administration under contract DE-NA0003525. This paper describes objective technical results and analysis. Any subjective views or opinions that might be expressed in the paper do not necessarily represent the views of the U.S. Department of Energy or the United States Government.

detonation. Predicting the violence of reaction is beyond the scope of the current work since violence mechanisms and processes are not fully understood [1]. The focus of the current paper is prediction of the time-to-ignition, the amount of decomposition gases, the pressurization of the confinement, and the state of the degraded energetic material (EM) at ignition.

Our cookoff models are based on solving the conductive energy equation and accounting for decomposition chemistry using a volumetric energy source. The models require temperature dependent thermal conductivity and specific heat as well as a kinetic mechanism that describes the time-dependent release of chemical energy. Phase changes are modeled as an energy sink using a normal distribution spread over a temperature range or mush zone that is defined by a solidus temperature (T_S) and a liquidus temperature (T_L). The distribution is sized so that 99% of the energy release occurs between T_S and T_L. Reaction rates are accelerated as the solid melts, or is dissolved in a solvent such as hot TNT (trinitrotoluene), or changes phase.

All thermophysical properties, including phase changes and latent enthalpies, are obtained from experimental data. However, the reaction mechanism is assumed to be universal with rates specific for each explosive. The reaction mechanism is based on four reactions: one for adsorbed gases, two for the explosive, and one for the binder. One of the explosive reactions describes condensed-phase dominated reactions that are independent of the pressure. The other explosive reaction accounts for gas-phase dominated reactions that are pressure sensitive.

The utility of the universal cookoff model is demonstrated by simulating four diverse explosives that contain HMX, TATB, RDX, and PETN; the explosives are PBX 9501 (95 wt% octahydro-1,3,5,7-tetranitro-1,3,5,7-tetrazoncine or HMX, 2.5 wt% nitroplasticizer or NP, and 2.5 wt% Estane®), PBX 9502 (95 wt% triaminotrinitrobenzene or TATB and 5 wt% chlorotrifluoroethylene/vinylidene fluoride binder or Kel-F), Comp-B (nominally 60 wt% hexahydro-1,3,5-trinitro-1,3,5-triazine or RDX and 40 wt% 2,4,6-trinitrotoluene or TNT), and PETN (pentaerythritol tetranitrate).

The model is used to predict ignition times as well as temperature and pressure profiles for several sets of cookoff data from different laboratories. The success of the universal cookoff model is attributed to 1) having good thermophysical properties, 2) using modified Arrhenius rate expressions where the activation energy is distributed with respect to the extent of reaction, and 3) accounting for pressure dependency.

Model and Parameters

Table 1 presents the "UNIVERSAL" cookoff model (UCM). Nomenclature and parameters are given in Table 2. The UCM is a solution of the conductive energy equation with a volumetric source term for the decomposition chemistry. The mechanism consists of four reaction steps representing 1) desorption of adsorbed gases such as moisture, 2) condensed-phase decomposition of the energetic material, 3) gas-phase decomposition of the energetic material, and 4) decomposition of the binder. Not all of these steps are necessary for every explosive. For example, some explosives do not have a binder (e.g. PETN), pristine explosives may not have adsorbed gases, etc.

Table 1. The "UNIVERSAL" cookoff model.[a]

Energy	$\rho_b C_b \frac{\partial T}{\partial t} = \nabla \cdot (k \nabla T) + \sum_{i=1,4} r_i h_{r,i} Mw_i$	(1)
Mechanism[b]	$S \xrightarrow{1} S_g$, Adsorbed gases (e.g. moisture)	(2)
	$E \xrightarrow{2} \alpha G_E + \beta C_E$, Condensed-phase dominant ($r_2 \neq \mathrm{f}[P]$)	(3)
	$E \xrightarrow{3} \alpha G_E + \beta C_E$, Gas-phase dominant ($r_3 = \mathrm{f}[P]$)	(4)
	$B \xrightarrow{4} \gamma G_B + \delta C_B$, Binder	(5)
Rates	$r_1 = A_1 T^{m_1} exp\left(\frac{-E_1 + \xi_1 \sigma_1}{RT}\right)[S]$	(6)
	$r_2 = A_2 \lambda_2 T^{m_2} \exp\left(\frac{-E_2 + \xi_2 \sigma_2}{RT}\right)[E]$	(7)
	$r_3 = A_3 \lambda_3 T^{m_3} \left(\frac{P}{P_o}\right)^{n_3} \exp\left(\frac{-E_3 + \xi_3 \sigma_3}{RT}\right)[E]$	(8)
	$r_4 = A_4 T^{m_4} \exp\left(\frac{-E_4 + \xi_4 \sigma_4}{RT}\right)[B]$	(9)
Species	$\frac{d[S]}{dt} = -r_1; \frac{d[S_g]}{dt} = r_1 ; \frac{d[E]}{dt} = -r_1 - r_3; \frac{d[G_E]}{dt} = \alpha(r_2 + r_3);$ $\frac{d[C_E]}{dt} = \beta(r_2 + r_3) ; \frac{d[B]}{dt} = -r_4; \frac{d[G_B]}{dt} = \gamma r_4; \frac{d[C_B]}{dt} = \delta r_4$	(10)
Distribution[c]	$\xi_1 = \mathrm{invnorm}\left(\frac{[S]}{[S_o]}\right); \xi_2 = \xi_3 = \mathrm{invnorm}\left(\frac{[E]}{[E_o]}\right); \xi_4 = \mathrm{invnorm}\left(\frac{[B]}{[B_o]}\right)$	(11)
Pressure	$P = \frac{nRT_{ave}}{V_g}$	(12)
Gas moles	$n = n_o + \int_V \left([S_g] + [G_E] + [G_B]\right) dV$	(13)
Gas temperature	$T_{ave} = \int_V \rho_b C_p T dV / \int_V \rho_b C_p dV$	(14)
Gas volume	$V_g = \int_V \phi dV$	(15)
Gas vol. fraction	$\phi = 1 - \left[S_f \rho_{co} (1 - \phi_o)/\rho_c\right]$	(16)
Condensed density	$\rho_c = \rho_{co}/(1 + \beta_v[T - T_o])$	(17)
Reacted solid fraction	$S_f = \sum_i Mw_i[\mathrm{i}]/\rho_{bo}$, where *i* is the condensed molar concentration	(18)

[a]Nomenclature is given in Table 2.

[b]Equilibrium product hierarchy from TIGER [2]. For example, RDX ($C_3H_6N_6O_6$) $\rightarrow 3N_2 + 2.46H_2O + 1.77CO_2 + 0.26CH_4 + 0.02H_2 + 0.97C$ or $E \rightarrow 7.51G_E + 0.97C$.

[c] "norminv" is the inverse of the standard normal cumulative distribution function.

The rate of decomposition of most energetic materials is strongly dependent on pressure. For example, the time-to-ignition, or ignition time, is significantly longer in vented systems than in sealed systems. Likewise, the ignition time in systems with excess gas volume is longer

than in systems with less gas volume. This behavior is modeled by using a condensed-phase reaction that dominates when the system is vented (see Eq. 3 and 7 in Table 1) and a gas-phase reaction that dominates when the system is sealed (see Eq. 4 and 8 in Table 1).

Pressure dependency typically implies that there is a significant gas phase reaction. However, tracking gas concentrations can be difficult for vented systems and is rarely measured. Yet, pressure is a relatively easy measurement and is proportional to the gas concentration. The effect of gas-phase dominated reactions is included in the UCM by multiplying the gas-phase dominant reaction rate by P/P_o raised to a power (see Eq. 8 in Table 1). The pressure exponent was determined in the current work using both vented and sealed data from the Sandia Instrumented Thermal Ignition (SITI) experiment.

The UCM includes a reaction for gas desorption (Eq. 2 and 6 in Table 1) as well as binder decomposition (Eq. 5 and 9 in Table 1). The initial increase in pressure caused by gas desorption can be significant for some explosives such as PBX 9502 decomposing in sealed systems. Energetic binders that decompose exothermically can lead to ignition in plastic bonded explosives such as PBX 9501 [3] and PBX 9404 (94 wt% HMX, 3 wt% nitrocellulose or NC, and 3 wt% plasticizer) [4].

Table 2. Nomenclature and model parameters.

Symbols	Description	Value	Units
$\mathrm{Ln}(A_1)$, $\mathrm{Ln}(A_2)$, $\mathrm{Ln}(A_3)$, $\mathrm{Ln}(A_4)$	Natural logarithm of the pre-exponential factors	RDX: 1, 35, 35, 1 9501: 35, 35, 35, 35 9502: 35, 35, 35, 1 PETN: 1, 35, 35, 1	$\mathrm{Ln}(s^{-1}K^{-n})$
α	Stoichiometric coefficient for gas products from explosive	RDX: 7.51 9501: 10.0 9502: 7.5 PETN: 10.0	none
β	Stoichiometric coefficient for condensed product from explosive	RDX: 0.97 9501: 1.6 9502: 3.9 PETN: 0.76	none
β_v	Volumetric thermal expansion coefficient	Comp-B: 1.64×10^{-4} 9501: 1.31×10^{-4} 9502: $(99+0.74T)\times10^{-6}$ PETN: 2.75×10^{-4}	$(m^3/m^3)K^{-1}$
B	Binder	Comp-B: binder (TNT) inert 9501: NP (nitroplasticizer) 9502: binder (Kel-F) inert PETN: none	none
$[B]$	Binder concentration	Comp-B: binder (TNT) inert 9501: initially $\omega_{np}\rho_{b,o}/M_{w,np}$ 9502: binder (Kel-F) inert PETN: none	$kgmol/m^3$
C_B	Carbon produced from binder	Symbol used in mechanism	none
C_E	Carbon produced from explosive	Symbol used in mechanism	none

$[C_E]$	Concentration of carbon produced from explosive	Initially 0	kgmol/m^3
C	Specific Heat (linearly interpolated, constant extrapolation)	T, K Comp-B: 273 1000; 350 1240; 477 1680 T, K 9501: 250 919; 700 2406 T, K 9502: 250 986; 700 2097 T, K PETN: 298 1090; 623 1760	Jkg^{-1}K^{-1}
C_b	Bulk specific heat	See "C" above	Jkg^{-1}K^{-1}
δ	Stoichiometric coefficient for condensed products from binder	RDX: binder (TNT) inert 9501: 1 (NVR) 9502: binder (Kel-F) inert PETN: no binder	none
E	Energetic material	Comp-B: RDX 9501: HMX 9502: TATB PETN: PETN	none
$[E]$	Energetic material concentration	Comp-B: initially $\omega_{rdx}\rho_{b,o}/M_{w,RDX}$ 9501: initially $\omega_{hmx}\rho_{b,o}/M_{w,HMX}$ 9502: initially $\omega_{tatb}\rho_{b,o}/M_{w,TATB}$ PETN: initially $\omega_{petn}\rho_{b,o}/M_{w,PETN}$	kgmol/m^3
E_1/R, E_2/R, E_3/R, E_4/R	Activation energies divided by R	RDX: 0 15920 22700 0 9501: 25500 19100 19100 20430 9502: 25500 17430 16860 0 PETN: 0 18220 19230 0	K
ϕ	Gas volume fraction	Field variable	m^3/m^3
ϕ_o	Initial gas volume fraction	$1-\rho_{bo}/\rho_{co}$	m^3/m^3
γ	Stoichiometric coefficient for gas products from binder	RDX: binder (TNT) inert 9501: 1 (NO_2) 9502: binder (Kel-F) inert PETN: no binder	none
$[G_B]$	Gas from binder	Initially 0	kgmol/m^3
$[G_E]$	Gas from explosive	Initially 0	kgmol/m^3
Comp-B reactions: $h_{f,i}$, where i= RDX, G, C	Heat of formation of i RDX→ 7.51G + 0.97C	69×10^6, -175×10^6, 0	Jkgmol^{-1}
PBX 9501 reactions: $h_{f,i}$, where i= S, Gs $h_{f,i}$, where i= HMX, G, C $h_{f,i}$, where i= NP, NVR, NO_2	Heat of formation of i: S→ G_S HMX→ 10G + 1.6C NP→ NVR + 4NO_2	-285.8×10^6, -241.8×10^6 75×10^6, -175×10^6, 0 -619×10^6, -1400×10^6, 34.2×10^6	Jkgmol^{-1}
PBX 9502 reactions: $h_{f,i}$, where i= S, Gs $h_{f,i}$, where i= TATB, G, C	Heat of formation of i: S→ G_S TATB→ 7.5G + 3.9C	-285.8×10^6, -241.8×10^6 75×10^6, -175×10^6, 0	Jkgmol^{-1}
PETN reactions: $h_{f,i}$, where i= PETN, G, C	Heat of formation of i PETN→ 10G + 0.76C	-593×10^6, -253.8×10^6, 0	Jkgmol^{-1}
Comp-B latent effects: $h_{latent,TNT\ melt}$ $h_{latent,RDX\ dissolution}$ $h_{latent,RDX\ melt}$	Latent enthalpies modeled thermodynamically using a normal distribution spread over a range defined by T_S, K and T_L, K.	T_S T_L h_{latent} TNT_{melt}: 350 360 $(1-\omega_{rdx})\times98450$ RDX_{dis}: 419 471 $\omega_{dis}\omega_{rdx}\times100000$ RDX_{melt}: 471 477 $(1-\omega_{dis})\omega_{rdx}\times148500$	J $kg_{Comp\text{-}B}^{-1}$
PBX 9501 latent effects: $h_{latent,HMX\ \beta\text{-}\delta}$ $h_{latent,HMX\ melt}$	Latent enthalpies	T_S T_L h_{latent} HMX β-δ: 441 447 $\omega_{hmx}\times33000$ HMX melt: 529 531 $\omega_{hmx}\times236000$	J kg_{9501}^{-1}
PETN latent effects: $h_{latent,PETN\ melt}$	Latent enthalpies	T_S T_L h_{latent} PETN melt: 529 531 $\omega_{petn}\times177000$	J kg_{petn}^{-1}
k Thermal conductivity (linearly interpolated, constant extrapolation)	Comp-B: T, K 1710 kgm^{-3} 440 0.2 447 0.3 9501: T, K 860 kgm^{-3} 1778 kgm^{-3} 441 0.12 0.33 447 0.11 0.21 9502: T, K 749 kgm^{-3} 1898 kgm^{-3} 300 0.10 0.70 400 0.13 0.55		Wm^{-1}K^{-1}

		500 0.13 0.48 520 0.15 0.47	
k	Thermal conductivity (linearly interpolated, constant extrapolation)	PETN T, K 230 kgm^{-3} 550 kgm^{-3} 1600 kgm^{-3} 1700 kgm^{-3} 413.0 0.038 0.079 0.216 0.229 415.5 0.040 1.486 1.5 1.5 417.5 0.442 1.892 1.9 1.9	$Wm^{-1}K^{-1}$
λ_2 (Comp-B)	Liquefaction rate accelerator	(1+0.5×(1+tanh((T-474)/2))×49)	none
λ_3 (Comp-B)	Dissolution rate accelerator	(1+0.5×(1+tanh((T-445)/4))×19)	none
$\lambda_2 = \lambda_3$ (9501)	Liquefaction rate accelerator	(1+0.5×(1+tanh((T-530)/2))×9)	none
$\lambda_2 = \lambda_3 = 0$ (9502)	Liquefaction rate accelerator	0	none
$\lambda_2 = \lambda_3$ (PETN)	Liquefaction rate accelerator	(1+0.5×(1+tanh((T-414)/2))×1)	none
$m_1 = m_4$	Steric factor for reaction 1 and 4	0 (Comp-B, 9501, 9501, PETN)	none
m_2	Steric factor for reaction 2	Comp-B: -0.8 9501: -0.6 9502: -2 PETN: 0	none
m_3	Steric factor for reaction 3	Comp-B: -0.8 9501: -0.7 9502: -2 PETN: -0.2	none
Comp-B reactions: $M_{w,i}$, where i= RDX, G, C	Molecular weight of species	222.1, 28, 12	kg/kgmol
9501 reactions: $M_{w,i}$, where i= S, Gs $M_{w,i}$, where i= HMX, G, C $M_{w,i}$, where i= NP, NVR, NO_2	Molecular weight of species	18, 18 296.2, 27.6, 12 319, 135, 46	kg/kgmol
9502 reactions: $M_{w,i}$, where i= S, Gs $M_{w,i}$, where i= TATB, G, C	Molecular weight of species	18,18 258.2, 28.2, 12	kg/kgmol
PETN reactions: $M_{w,i}$, where i= PETN, G, C	Molecular weight of species	316.1, 30.7, 12	
n	Moles of gas	Field variable (Eq. 13)	kgmol
n_3	Pressure exponent for reaction 3	Comp-B: 0.8 (sealed) and 0 (vented) 9501: 0.6 (sealed) and 0 (vented) 9502: 1.0 (sealed) and 0 (vented) PETN: 0.2 (sealed) and 0 (vented)	none
normsinv	Inverse of the standard normal distribution	function	none
P	Pressure	Initially 0	MPa (psig)
P_o	Initial pressure	0.1 (14.7) ODTX 0.08 (12.1) SITI	MPa (psia)
ρ	Bulk density	Field variable	kgm^{-3}
$\rho_{b,o}$	Initial bulk density	ODTX SITI Comp-B: 1670 1710 9501: 1790 860, 1580, 1780 9502: 1900 750, 1890 PETN: 1680 550, 1700	kgm^{-3}
ρ_c	Condensed density	Field variable (Eq. 17)	kgm^{-3}
$\rho_{c,o}$	Initial condensed density (TMD)	Comp-B: 1742 9501: 1860 9502: 1942 PETN: 1780	kgm^{-3}
R	Gas constant	0.08206 8314	m^3 atm $kgmol^{-1}K^{-1}$ J $kgmol^{-1}K^{-1}$

σ_1/R, σ_2/R, σ_3/R, σ_4/R	Distribution parameters	Comp-B: 0, -1500, 500, 0 9501: 2500, -1000, -1000, -400 9501: 2500, -1000, -1300, 0 PETN: 0, -600, -200, 0	K
S	Sorbed gas	Comp-B: none 9501: water 9502: water PETN: none	none
$[S]$	Sorbed gas concentration	Comp-B: 0 9501: initially $\omega_s\rho_{b,o}/M_{w,s}$ 9502: initially $\omega_s\rho_{b,o}/M_{w,s}$ PETN: 0	kgmol/m^3
S_g	Desorbed gas	Comp-B: none 9501: water vapor 9502: water vapor PETN: none	none
$[S_g]$	Desorbed gas concentration	Comp-B: none 9501: initially 0 9502: initially 0 PETN: none	kgmol/m^3
S_f	Reacted solid fraction	Field variable (Eq. 18)	kg/kg
T	Temperature	Field variable (Eq. 1)	K
T_{ave}	Average gas temperature	Global variable (Eq. 14)	K
T_L	Temperature at the end of a phase change	See h_{latent} for values	K
T_o	Initial temperature	ODTX: 300 K SITI: 294.1±2.3 K	K
T_S	Temperature at the beginning of a phase change	See h_{latent} for values	K
V_{ex}	Excess gas volume	ODTX: 0.0457×10^{-6} (gaps) + 0.00222×10^{-6} (Al expansion) SITI large ullage: 19.76×10^{-6} SITI small ullage: 2.39×10^{-6}	m^3
V_g	Gas volume	Global variable from Eq. 15	m^3
V_{EM}	Volume of the energetic material	ODTX: 1.073×10^{-6} SITI pressed pellets: 12.87×10^{-6}	m^3
ω Initial mass fractions	Comp-B: $\omega_s = 0$, $\omega_{rdx} = 0.63$, $\omega_{tnt} = 0.37$ 9501: $\omega_s = 0.005$, $\omega_{hmx} = 0.95(1-\omega_s)$, $\omega_{NP} = \omega_{estane} = 0.025(1-\omega_s)$ 9502: $\omega_s = 0.0015$, $\omega_{tatb} = 0.95(1-\omega_s)$, $\omega_{kelf} = 0.05(1-\omega_s)$ PETN: $\omega_s = 0$, $\omega_{petn} = 1$		kg/kg
ω_{dis}	Mass fraction of dissolved RDX in hot TNT at 473 K	0.50	kg/kg
ω_{estane}, ω_{hmx}, ω_{kelf}, ω_{NP}, ω_{petn}, ω_{rdx}, ω_s, ω_{tatb}, ω_{tnt}	Initial mass fraction of Estane®, HMX, Kel-f, nitroplasticizer, PETN, RDX, sorbed gases, TATB, and TNT	See ω for values for Comp-B, 9501, 9502, and PETN	kg/kg
ξ	normsinv	Field variable	none

The thermal conductivities were obtained by matching finite element calculations with measured temperatures in the SITI tests. The specific heat for Comp-B was determined by doing a mass fraction weighted average of the temperature dependent specific heat of TNT and RDX as measured by Baytos [5]. Baytos also measured the specific heat of Comp-B3 (60:40

RDX:TNT), which we did not use since the values above the melting point were significantly higher than either the TNT or RDX values. The specific heats for PBX 9501, PBX 9502, and PETN were taken from [3], [6], and [7], respectively.

The success of the universal cookoff model is attributed to the non-Arrhenius form of the rate expressions. For example, the distributed activation energy model can be used to either accelerate or decelerate a reaction, which is reminiscent of autocatalytic reactions and diffusion reactions, respectively. Acceleration is achieved when the distribution parameters are negative ($\sigma < 0$). Deceleration occurs when the distribution parameters are positive ($\sigma > 0$). Explosives usually have a long induction period, where chemistry is slow and the dissipation is fast. As the explosive degrades, the rates begin to accelerate until ignition occurs. In contrast, reactions such as desorption of moisture is a diffusion limited process, which starts out fast and then decelerates as the moisture evolves.

Phase changes are usually endothermic and are modeled as energy sinks using a normal distribution sized so that 99% of the energy release occurs between T_S and T_L. Reaction rates are usually faster in the liquid phase than in the solid phase as discussed by Manelis et al. [8]. Rate acceleration is modeled by the rate enhancement factors, λ, which can be attributed to physical changes in the explosive such as liquefaction or even dissolution of RDX in hot liquid TNT.

Experiments

Calibration and validation of the UCM is done using the SITI and ODTX (one-dimensional time-to-explosion) experiments, respectively. The SITI experiment, shown in Fig. 1, is used to obtain the thermal conductivity and the reaction rate parameters. The SITI experiment consists of a 2.54 cm diameter by 2.54 cm tall cylinder of explosive confined by aluminum that is ramped to a set point temperature (T_{sp}) in 10 min and held until ignition. Internal temperatures are measured using type K 127 μm diameter thermocouples located at various radial position in the center of the explosive cylinder as shown in Fig. 1.B. Pressure is measured using a Kulite HEM-375-2000A pressure transducer. More details regarding the SITI experiments can be found in [3, 6, 7, 9].

Only a few of the SITI experiments were used for calibration, and the remaining experiments were used to validate the model. ODTX data from Lawrence Livermore National Laboratory are used to further validate the UCM. The ODTX experiment considers a 1.27 cm diameter sphere of explosive confined by two aluminum anvils using a hydraulic press with a

holding pressure of 1500 bars. The two cylindrical anvils, with two hemispheres machined to accommodate the spherical PBX, are preheated to a given temperature. The ignition time is recorded as the time the anvils are closed to the time the anvils mechanically fail, typically by thermal ignition of the explosive. Details of the ODTX experiment can be found in references [4, 10, 11].

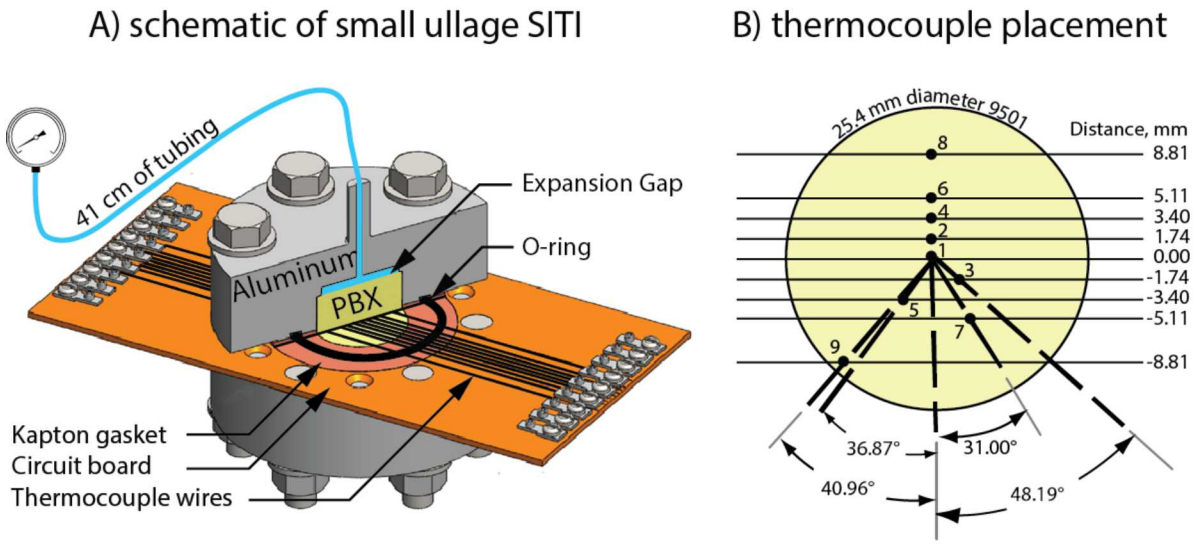

Figure 1. Schematic of A) SITI with B) thermocouple locations.

Cookoff Predictions using Comp-B, PBX 9501, PBX 9502, and PETN

Figure 2 presents comparisons between predicted (orange lines) and measured (green lines) internal temperature and pressure for Comp-B, PBX 9501, PBX 9502, and PETN, respectively. Temperatures are predicted at the thermocouple bead locations shown in Fig. 1.B. Pressures were measured in the sealed experiments with a pressure transducer. Figure 2 shows the ability of the UCM to predict the effects of melting (see Fig 2.A for TNT melt and Fig 2.D for PETN melt), polymorphic phase change (see Fig. 2.B for β-HMX to δ-HMX phase change), and exothermic binder decomposition (see Fig. 2.B).

Figure 3 shows how well the UCM predicts ignition times for both sealed and vented SITI experiments [3, 6, 7, 9] and sealed ODTX experiments [4, 10, 11, 12] for Comp-B, PBX 9501, PBX 9502, and PETN. The UCM model adequately predicts ignition time provided the model is calibrated with sufficient vented and sealed data preferably at several densities. More vented data is needed for the PETN model, which has been difficult to obtain due to complications associated with melting and boiling. Using larger diameter vent holes with more ullage should help reduce experimental uncertainty for these future experiments.

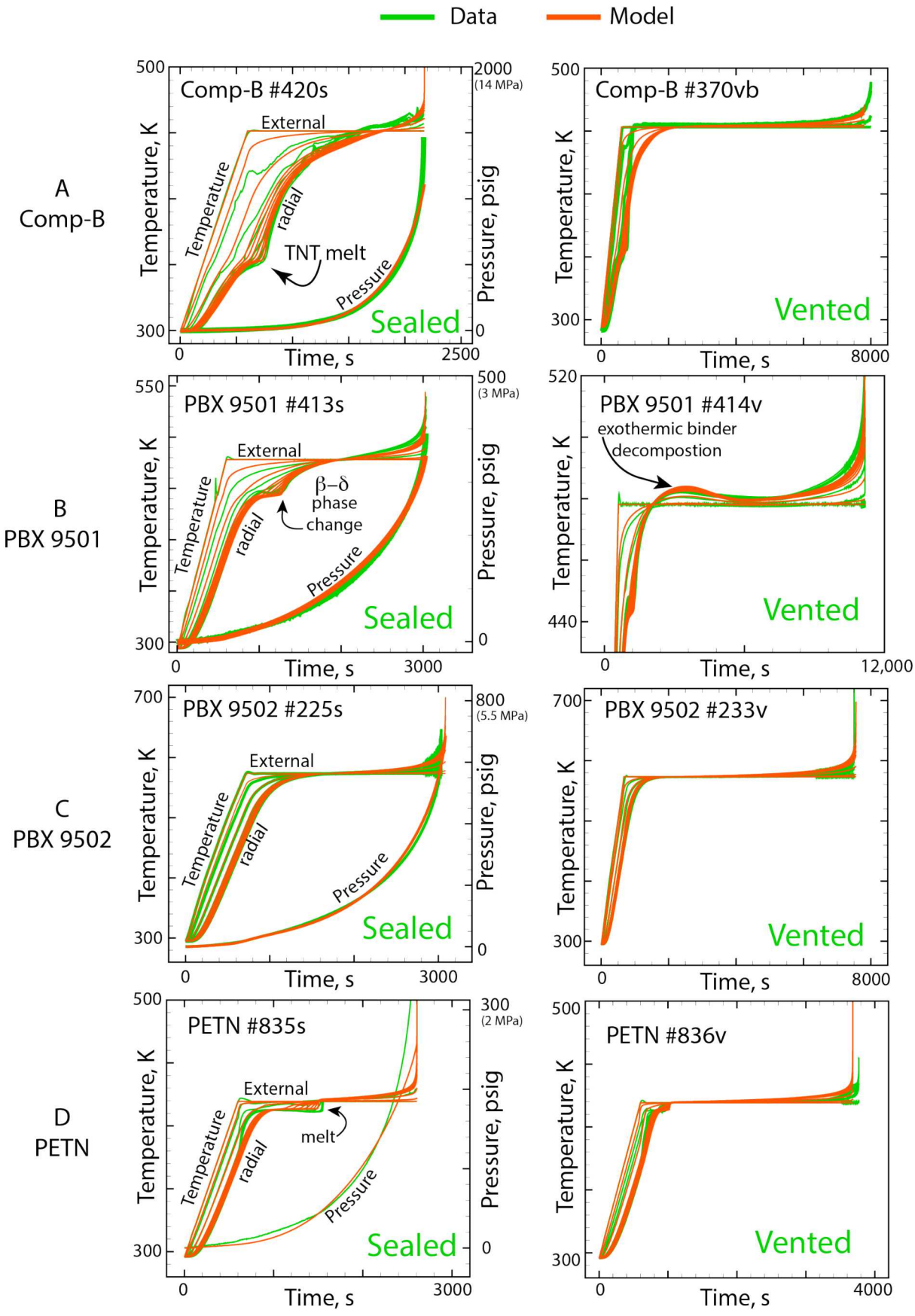

Figure 2. Predicted (orange lines) and measured (green lines) temperatures and pressures during cookoff of vented and sealed A) Comp-B, B) PBX 9501, C) PBX 9502, and D) PETN in the SITI experiments.

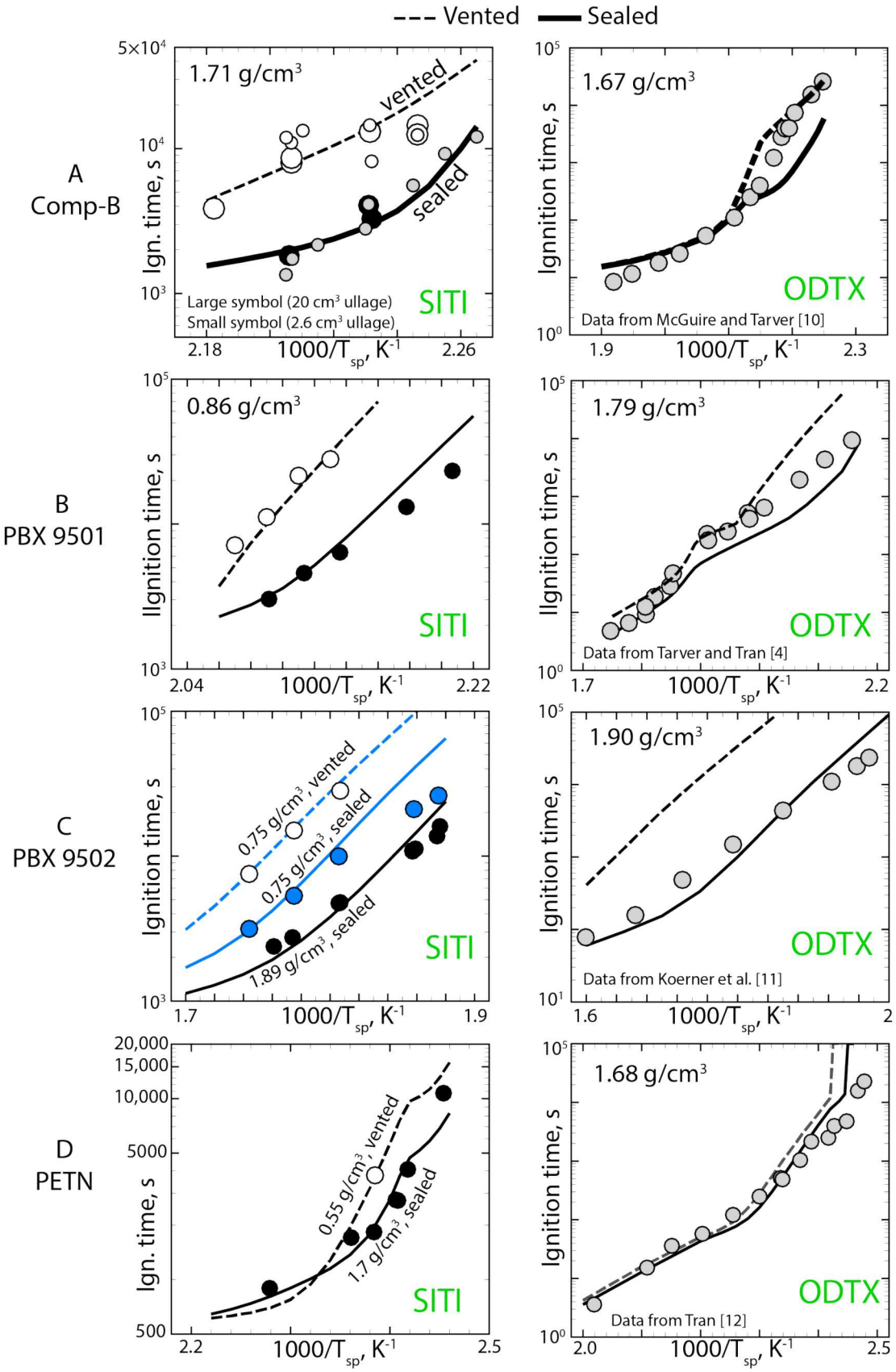

Figure 3. Predicted (lines) and measured (symbols) ignition times for vented (dashed lines) and sealed (solid lines) A) Comp-B, B) PBX 9501, C) PBX 9502, and D) PETN in the SITI experiments [3, 6, 7, 9] and the ODTX experiments [4, 10, 11, 12].

Summary and Conclusions

We have developed a "UNIVERSAL" cookoff model that was calibrated with cookoff data for Comp-B, PBX 9501, PBX 9502, and PETN. The success of the model was attributed to rate expressions that can be calibrated to rates that range from diffusion limited to autocatalytic behavior. This form of the rate expression allows pressure to be predicted accurately, allowing predictions of vented and sealed systems. Model predictions demonstrated adequate predictions of spatial temperature, pressure, and ignition times for four diverse explosives. Our predictions were as good as models with uniquely different mechanisms.

Acknowledgements

Partial support of this work was from the joint DoD/DOE Munitions Program. We thank Shane Snedigar for running all of the SITI experiments; Sophia Lefantzi, Leanna Minier, Darcie Farrow, and Clint Hall for their constant interest and enthusiasm regarding our experimental and modeling activities. Reviewers, David Kittell and Stephanie Coronel, are also appreciated.

References

[1] M. D. Cook, C. Stennett and M. L. Hobbs, "Development of a small scale thermal violence test," in *16th International Detonation Symposium*, Cambridge, 2018.

[2] M. L. Hobbs, R. G. Schmitt, H. K. Moffat and Z. Lawless, "JCZS3--An Improved Database for EOS Calculations," in *Proceedings of the 16th International Detonation Symposium*, Cambridge, 2018.

[3] M. L. Hobbs, M. J. Kaneshige and W. W. Erikson, "Modeling the measured effect of a nitroplasticizer (BDNPA/F) on cookoff of a plastic bonded explosive (PBX 9501)," *Combustion and Flame,* vol. 173, pp. 132-150, 2016.

[4] C. M. Tarver and T. D. Tran, "Thermal decomposition models for HMX-based plastic bonded explosives," *Combustion and Flame,* vol. 137, pp. 50-62, 2004.

[5] J. F. Baytos, "Specific Heat and Thermal Conductivity of Explosives, Mixtures, and Plastic-Bonded Exposives Determined Experimentally," LA-8034-MS Informal Report, UC-45, Los Alamos Scientific Laboratory, Los Alamos, 1979.

[6] M. L. Hobbs and M. J. Kaneshige, "Ignition experiments and models of a plastic bonded explosive (PBX 9502)," *The Journal of Chemical Physics,* vol. 140, p. 124203, 2014.

[7] M. L. Hobbs, W. B. Wente and M. J. Kaneshige, "PETN Ignition Experiments and Models," *J. Phys. Chem. A,* vol. 114, pp. 5306-5319, 2010.

[8] G. B. Manelis, G. M. Nazin, Y. I. Rubtsov and V. A. Strunin, Thermal Decomposition and Combustion of Explosives and Propellants, London and New York: Taylor & Francis, 2003.

[9] M. L. Hobbs, M. J. Kaneshige, W. W. Erikson, J. A. Brown, M. U. Anderson, S. N. Todd and D. G. Moore, "The Effects of Temperature, Pressure, and Flow on Cookoff of a Melt-castable Explosive (Comp-B)," *Manuscript submitted for publication,* 2019.

[10] R. R. McGuire and C. M. Tarver, "Chemical Decomposition Models for the Thermal Explosion of Confined HMX, TATB, RDX, and TNT Explosives," in *Seventh Symposium (International) on Detonation*, Annapolis, 1981.

[11] J. Koerner, J. Maienschein, A. Burnham and A. Wemhoff, "ODTX Measurements and Simulations on Ultra Fine TATB and PBX 9502," in *North American Thermal Analysis Society 35th Annual Conference*, East Lansing, 2007.

[12] T. D. Tran, Private Communication, Lawrence Livermore National Laboratory, 2008. Data in C. M. Tarver, T. D. Tran, R. E. Whipple, "Thermal Decomposition of Pentaerythritol Tetranitrate," *Propellants, Explosives, Pyrotechnics*, vol. 28, pp. 189-193, 2003.